

Plant hydraulic and stomata control explains the response of a seasonal tropical forest to water stress over multiple temporal scales

Detto et al.

Department of Ecology and Evolutionary Biology, Princeton University, Princeton, NJ

Smithsonian Tropical Research Institute, Balboa, Panama, Panama

Key words: Tropical forest, carbon cycles, gross primary productivity, evapotranspiration, water stress, El Nino, stomata control, plant hydraulics.

Running title (45 characters included space): response to water stress of a seasonal tropical forest

**Contact information*

e-mail: mdetto@princeton.edu

phone: +1-609-258-6886

Target Journal: Global Change Biology (up to 8000 words in length including Introduction, Materials and Methods, Results, Discussion, and Acknowledgements)

Abstract: (Limited to 300 words, still in progress)

Many tropical regions are experiencing an intensification of drought, with increasing severity and frequency of the events. However, the forest ecosystem response to these changes is still highly uncertain. It has been hypothesized that on short time scales (from diurnal to seasonal), tropical forests respond to water stress by physiological controls, such as stomata regulation and phenological adjustment, to control increasing atmospheric water demand and cope with reduced water supply. However, the interactions among biological processes and co-varying environmental factors that determine the ecosystem-level fluxes are still unclear. Furthermore, climate variability at longer time scales, such as that generated by ENSO, produces less predictable effects, which might vary among forests and ecoregions within the tropics.

This study will present some emerging patterns of response to water stress from five years of observations of water, carbon, and energy fluxes on the seasonal tropical forest in Barro Colorado Island (Panama), including an increase in productivity during the 2015 El Niño. We will show how these responses will depend critically on the combination of environmental factors experienced by the forest along the seasonal cycle. These results suggest a critical role of plant hydraulics in mediating the response to water stress on a broad range of temporal scales, including during the wet seasons when water availability is not a limiting factor. The study also found that the response to large-scale drought events is contingent and might produce a different outcome in different tropical forest areas.

Introduction

Fast rates of carbon recycle, large stock in living biomass and soil make tropical forests central players of the terrestrial carbon budget (Houghton 2005; Beer *et al.* 2010; Pan *et al.* 2011). Climate change can alter basic forest functions with potentially long-term negative impacts on carbon sequestration, storage, and maintenance of biodiversity.

Many tropical regions are experiencing intensifications of droughts in the form of higher water atmospheric demand (Barkhordarian *et al.* 2019), increasing frequency and duration of dry spells (Marengo *et al.* 2009), increasing frequency and severity of large scale events (Cai *et al.* 2014) and a shift of climate seasonality (Feng *et al.* 2013). In regions not generally associated with drought stress, such as tropical rainforests, these changes might cause substantial alterations of ecosystem dynamics (Meir *et al.* 2015). Therefore, besides direct human impacts from deforestation and land-use change, the fate of tropical forests will be determined by their response to increasing droughts (Corlett 2016; Brodrribb *et al.* 2020).

Seasonally dry tropical forests offer a great opportunity to study these responses because species have adapted strategies to cope with periods of limited water supply (Wright & van Schaik 1994). For example, leaf shedding (hydraulic fuse) slows water loss, stabilizes plant water potentials, and protects against cavitation-induced loss of stem hydraulic conductivity (Tyree *et al.* 1993). However, although the hydraulic fuse is well supported in seasonal tropical forests, also in response to El Niño Southern-Oscillation (ENSO) (Detto *et al.*, 2018), it is not universally effective at stabilizing plant water potential (Wolfe *et al.* 2016), and it cannot operate at short time scales (e.g., diurnal, daily or weekly). Conversely, more extreme drought avoidant strategies, in which the whole crown is left leafless for the entire duration of the dry season (dry deciduousness), save costly adaptation to water stress, such as embolism-resistant xylem and deep and extended root systems, but sacrifice productivity.

Several empirical and theoretical studies have recently pointed out the importance of plant hydraulics in understanding the response of tropical plants to droughts (Poorter *et al.* 2010; Xu *et al.* 2016; Barros *et al.* 2019; Bartlett *et al.* 2019; Powers *et al.* 2020). Plant hydraulics apply significant constraints on ecosystem productivity, affecting several physiological processes, in particular stomata regulation. Similarly to the hydraulic fuse, plants actively control stomata aperture to reduce tension on the xylem that could cause irreparable damage or costs to repair and rebuilt compromised tissues (e.g., refill of embolized vessels) that would exceed the benefits of fixed carbon (Katul *et al.* 2010; Sperry *et al.* 2016; Wolf *et al.* 2016). Stomata respond to several environmental stimuli, including ambient CO₂, light, vapor pressure deficit, and leaf water potential, and interact with other physiological processes such as thermoregulation (Still *et al.*, in prep.). Consequently, the combined effect of increasing water atmospheric demand and light and reduced water supplies are hard to predict (Jarvis 1976). Furthermore, it is unclear how this short-term and leaf-level mechanism contributes to the whole ecosystem-level response of tropical forests to drought on multiple temporal scales.

Empiricists have investigated this question with physiological studies based on leaf gas exchange, sapflow and functional traits (e.g., Santiago *et al.* 2004; Eller *et al.* 2018; Santos *et al.* 2018; Grossiord *et al.* 2019). However, although they have identified a critical role of stomata control and plant hydraulics

in regulating CO₂ and water exchange that is consistent with theory, observed patterns remain still hard to predict. For example, two comparative studies, one in the Panamanian rainfall gradient and the other in the Amazon, found no differences in stomata response among forests with contrasting precipitation regimes (Barros *et al.* 2019; Wu *et al.* 2020). Barros *et al.* (2019) explained the lack of pattern with the ability of plants in the drier forest to tolerate lower xylem water potentials because of hydraulic traits that convey greater xylem embolism resistance. Wu *et al.* (2020) concluded that plant hydraulics was not important for predicting stomatal response in these forests.

At the ecosystem level, gross primary productivity (GPP) is expected to decline during the driest months of the seasonal cycle. However, studies based on eddy covariance flux towers across the Amazonian rainforest, with different intensities and durations of the dry season, have shown no or little seasonality in GPP (Carswell *et al.* 2002; Keller *et al.* 2004) or even an inverse pattern with higher GPP in the dry season (Goulden *et al.* 2004; Green *et al.* 2020). A comparative study in Southern China shows strong seasonality of GPP in a subtropical forest but no seasonality in a tropical forest, despite the two sites experiencing similar seasonal rainfall patterns (Yan *et al.* 2013). The limited eddy covariance data in the tropics have also produced conflicting views on the impacts of droughts induced by ENSO, with reports of negative and positive effects on GPP (Olchev *et al.* 2015; Cavaleri *et al.* 2017). Similarly, satellite observations found different responses to seasonal and interannual drought (Yang 2018; Zhu *et al.* 2018; Qian *et al.* 2019; Green *et al.* 2020). For example, Green *et al.* (2020) found an increase in the Amazon rainforest photosynthesis with increasing atmospheric dryness, a pattern explained by a change in canopy properties, a hypothesis previously explored by Wu *et al.* (2016).

These results suggest that the coupled hydraulic-stomata system responds to multiple environmental factors and is mediated by other physiological controls. Furthermore, it is important to consider that climatic drivers often co-varies at several temporal scales. Periods of low water supply and high atmospheric demand correspond to periods of high solar irradiance due to clear sky conditions, which might compensate for the negative effect of water stress in high leaf area forests. As the covariation among environmental factors varies among tropical regions and across time scales, the response to drought might be contingent on a particular forest and a particular event.

These uncertainties reflect in our inability to satisfactory model ecosystem fluxes in tropical forests, especially seasonal and interannual variability, and to predict the response to water stress (Restrepo-Coupe *et al.* 2017; Huang *et al.* 2020) and call for a better understanding of the mechanisms driving these responses on a broad range of temporal scales and in different forests (Christoffersen *et al.* 2014; Bonal *et al.* 2016; Koven *et al.* 2019). In this study, we use five years of eddy covariance CO₂ and H₂O fluxes above an old-growth tropical forest in central Panama to quantify the response to water stress on a range of temporal scales, including diurnal cycle, intraseasonal variability (e.g., dry spells), seasonal cycles and interannual variability driven by the 2015-2016 El Niño event. We show that, although the reduction of canopy conductance is higher during the dry season, soil moisture strongly mediated the response of stomata to atmospheric drivers during both seasons. We also found an increase in forest productivity during the 2015 El Niño year caused by two dry spells during the wet season, which enhanced solar radiation without reducing soil moisture below critical levels. The increase in GPP during

a year of water stress is consistent with a concomitant increase in light availability during a greening phase of the forest.

Recent modeling studies in this forest have focused on identifying plant traits to improve the representation of tropical forest structure and successional dynamics in Earth System Models (Koven *et al.* 2019; Martínez Cano *et al.* 2020; Rüger *et al.* 2020). However, limited attention has been devoted to connecting models to empirical patterns of forest response to water stress over multiple time scales, despite simulated evapotranspiration (ET) and GPP are quite sensitive to plant hydraulic traits (Fang *et al.* 2021). Here we do so by coupling a multilayer photosynthetic model with plant hydraulics linked through a stomata control. We formulate the stomata control as an optimization problem where plants maximize carbon gain, the difference between photosynthesis and the direct costs of water stress. We demonstrate that the empirical patterns can be predicted by a tradeoff between parameters that convey the efficiency of water transport (e.g. maximum hydraulic conductivity) vs. parameters that reduce the cost of water stress.



Figure 1. Images taken by a phenocam (NetCam SC, StarDot Technologies) located on the top plateau on Barro Colorado Island in the middle of the 2015 dry season and during the beginning of the 2015 wet season. The images show several leafless deciduous trees (left panel) completely recovered just before the two anomalous dry spells hit the island during the El Niño event. Note how the vegetation looks, in general, much brighter green in the right picture despite different illumination conditions.

Materials and Methods

Site description

Barro Colorado Island (BCI; 9° 9' N, 79° 50' W) is a 16 km² island in Lake Gatun, Panama, disconnected from the mainland after the Panama Canal construction. Annual rainfall averages 2640 mm, with a distinct dry season between mid-December and mid-April. The mean annual temperature is 26° C, with

minimal seasonal variation (Windsor 1990). BCI supports tropical moist forest in the Holdridge Life Zone System and tropical monsoon climate in the Köppen–Geiger classification system.

BCI harbors more than 1,300 known plant species (Croat 1978), about 480 tree and shrub species, and 265 species of lianas and vines. Among 211 tree species that can attain a height of 10 m, about ~12% lose all or nearly all their leaves for at least part of the dry season (Croat, 1978) – see Fig. 1. The most common canopy species found in the near footprint of the experimental sites include, among others: *Gustavia superba*, *Hura crepitans*, *Inga pezizifera*, *Platypodium elegans*, *Pseudobombax septenatum*, *Spondia radlkoferi*, *Tabebuia guaycan*, *Tabebuia rosea*, *Trichila Tuberculata*, and *Virola surinamensis*.

Data collection and processing: Turbulent fluxes and meteorological variables were measured from a 41 m Eddy Covariance (EC) flux tower located on the top plateau of the island at about 140 m ASL from July 2012 to August 2017. The eddy covariance system included a sonic anemometer (CSAT3, Campbell Scientific) and an open-path infrared CO₂/H₂O gas analyzer (LI-7500A, LiCOR Bioscience). Hi-frequency (10Hz) measurements were acquired by a datalogger (CR1000, Campbell Scientific) and stored on a local PC. Additional environmental variables used in this study include rainfall (Tipping Bucket Rain Gages TB4, Hydrological Services), temperature and relative humidity (HC2S3, Rotronic), solar radiation (CMP11, Kipp&Zonen), upwelling and downwelling shortwave and longwave radiations (CNR1, Kipp&Zonen), direct and diffuse PAR (BF5, Delta-T Devices), and canopy temperature obtained from five infrared thermometers (SI-131, Apogee Instruments) pointing the crowns of the four nearest canopy trees surrounding the tower. Three time domain reflectometers (CS616, Campbell Scientific) were installed vertically around the tower and calibrated with gravimetric soil moisture samples taken in different moisture regimes in the proximity of the probes (Suppl. Mat. Fig. S7). Three additional probes were installed horizontally in 2016 at 10, 40 and 100 cm depths. CO₂ profiles within the canopy were measured in two periods, from 2014-12-11 to 2015-01-21 and from 2016-08-01 to 2016-10-11, using a closed-path gas analyzer (LI-8100A) equipped with a multiplexer (LI-8150). The air was sampled at 2, 10, 20 and 30 m from the ground. Because the 10, 20 and 30 m levels gave very similar values, in 2016 the air was sampled only at 2 and 30 m.

Data were processed with a custom program using a standard routine described in (Detto *et al.* 2010). QA/QC criteria follow guidelines for removing erroneous values (Mauder *et al.* 2013) and include not ideal turbulent conditions, periods during and immediately after rain, outliers of several scalar statistics, poor energy budget closure and light response, stationary check, and known sensor malfunctioning (See Supplementary Table S1 and Fig S1 for QA/QC criteria and the percent of gaps by month).

GPP was derived from net ecosystem exchange (NEE) daytime values by adding the corresponding mean daily ecosystem respiration (RECO). Two approaches were implemented: in the first, RECO was obtained as the intercept of the light response curve (Lasslop *et al.* 2010), and in the second, by using mean nighttime fluxes. Both methods were performed on a ±15-days moving window for values of friction velocity >0.4 m/s to minimize flux underestimations (Fig. S3). Because of relatively small variation in air temperature and lack of temperature dependence of soil respiration (Rubio & Detto 2017), the temperature was not included as a covariate for estimating RECO. The two methods provided similar results, but the first method yielded higher values (Fig. S3), more consistent with manual and automated soil chamber measurements available for the same period in the tower's footprint (Rubio & Detto 2017).

Nighttime fluxes and RECO underestimations are common problems in tall and dense forests, even in sites, like BCI, that are well exposed to meteorological winds (Speckman *et al.* 2015). For these reasons, nocturnal CO₂ fluxes were not used further in this study.

Data analyses:

In order to compute daily and monthly time-integrated budgets (for Fig. 2), gaps were filled using an Artificial Neural Network (Papale & Valentini 2003) with hydro-meteorological inputs as predictors (soil moisture, various radiation components, temperature, VPD, and air pressure). The data were randomly divided into a training set (70%), a validation set (15%), and a test set (15%). A two-layer feed-forward network with 10 sigmoid hidden neurons and linear output neurons was trained using the Levenberg-Marquardt algorithm until the mean square error (MSE) of the validation set stop improving (Hagan & Menhaj 1994). Performance, in terms of MSE, was evaluated using the test set at the end of the training. This procedure was repeated 100 times to produce 100 estimates of GPP. Training multiple times generates different results due to different initial conditions and random sampling of the three sets. The ensemble was obtained as a weighted average from the 100 ANN predictions using the reciprocal of MSE of the test set as weights. For subsequent analyses, data were not gap-filled; instead, all analyses relied only on screened observations.

Canopy conductance, g_c , is often computed by inverting the Penman-Monteith equation (Monteith J.I. 1965) and solving for the reciprocal canopy resistance, r_c , (Novick *et al.* 2016; Green *et al.* 2020; Fang *et al.* 2021). The availability of the direct measurements of canopy temperature, allows implementing a more refined scheme that overcomes some of the implicit assumptions of the Penman equation (Brutsaert & Sugita 1991; Crago & Qualls 2014). We coupled bulk transfer functions of sensible heat (H , W m⁻²) and latent heat (λE , W m⁻²):

$$(1a) \quad H = \rho_a c_p \frac{t_c - t_a}{r_{ah}}$$

$$(1b) \quad \lambda E = \frac{\rho_a c_p e_s(t_c) - e_a}{\gamma r_{aq} + r_c}$$

where t_c and t_a are canopy and air temperature, respectively, $e_s(t_c)$ and e_a are the water vapor pressure (Pa) in the leaf stomata cavities and the air, respectively. The air in the intercellular space was considered at saturation and was expressed as a function of canopy temperature t_c from the Clausius–Clapeyron relation. r_{ah} and r_{aq} are the bulk aerodynamic resistances (s m⁻¹) for sensible heat and water vapor transfer and r_c is the canopy resistance (s m⁻¹). ρ_a is air density (g m⁻³), c_p is the specific heat capacity of air (J g⁻¹ K⁻¹) and γ the psychrometric constant (Pa K⁻¹). By combining (1a) and (1b), assuming $r_{ah} = r_{aq}$, canopy conductance, g_c (mol m⁻² s⁻¹), can be computed as:

$$(2) \quad g_c = \frac{\rho_a}{m_a} r_c^{-1} = \frac{1}{m_a c_p B_o} \frac{H}{\frac{e_s(t_c) - e_a}{\gamma} - (t_c - t_a)}$$

where $B_o = H/\lambda E$ is the Bowen ratio and m_a the molar mass of moist air (g mol⁻¹). All the terms in the RHS of (2) are measured directly from the tower. It should be noted that the bulk transfer formulations (Eqs 1), which imply a big-leaf representation of the forest, include contributions from soil and other

sources (e.g., condensation and evaporation of rainfall leaf interception). Consequently, g_c should be more correctly referred to as surface or ecosystem conductance and interpreted as a whole ecosystem property (Novick et al., 2016). At our site, little energy reached the forest floor because LAI is around 6 (Wirth *et al.* 2001; Detto *et al.* 2018), as also suggested by small fluctuations in soil temperature and small values of soil heat flux, which contributes less than 5% of net radiation (Supplementary Material - Fig S6). Furthermore, we excluded from the analyses periods during and immediately after rain events and early morning to minimize contributions to evapotranspiration from the soil, condensation, and leaf interception.

The response of g_c to vapor pressure deficit ($D = e_s(t_a) - e_a$) and the role of soil moisture was explored using the optimal stomatal model of Medlyn *et al.* (2011)

$$(3) \quad g_c = g_0 + \left(1 + \frac{g_1}{\sqrt{D}}\right) \frac{GPP}{c_a}$$

where c_a is the ambient CO₂ concentration, assumed constant and equal to 400 ppm, and g_0 and g_1 are empirical parameters. As the term $\frac{g_1}{\sqrt{D}}$ is typically >1, the model predicts a close linear relationship between g_c and $\frac{1}{\sqrt{D}} \frac{GPP}{c_a}$ (Medlyn *et al.* 2011). For this analysis, data were binned in eight soil moisture quantiles, and the relationship between g_c and $\frac{1}{\sqrt{D}} \frac{GPP}{c_a}$ was computed with a non-parametric regression using a Gaussian kernel (Watson 1964). Analyses were performed for wet and dry seasons independently. To minimize uncertainty in the computation of g_c associated with small fluxes, the analysis was limited to periods with solar radiation and latent heat >100 W m⁻².

In the last analysis, we computed the light use efficiency and the water use efficiency by regressing GPP against PAR and evapotranspiration. We used a two-parameters Michaelis–Menten model for the light use efficiency and a quadratic polynomial for the water use efficiency and fitted the models using nonlinear least square.

Most of the analyses were conducted separately for wet and dry seasons. The beginning of the dry season was defined from the first dry spell between December and January, when surface soil moisture dropped below 0.35. Analogously, the beginning of the wet season was defined from the first rain occurring between April and May when soil moisture raised above 0.35. All analyses were performed in Matlab (R2019a).

Model description

The model comprised three modules: *i*) a canopy radiative transfer model, *ii*) a leaf photosynthesis and, *iii*) a stomata optimization. As the focus of the model is on the link between plant hydraulics and canopy conductance, we report only the equations for the stomata optimization and verbally describe the other two modules. A complete analytical description of the model is provided in Appendix 2.

i) The radiative transfer model used a two-stream approximation to represent the penetration, absorption, and scattering of direct and diffuse radiations (both downward and upward) through the canopy profile (Meador & Weaver 1980; Pinty *et al.* 2006). Sunlit and shaded leaves were treated differently to represent the horizontal heterogeneity of the light environment within each layer

(Norman 1980). The absorption and scattering coefficients were parameterized from leaf optical properties in the PAR region (reflectance and transmittance) and leaf angle distributions (Yuan *et al.* 2017). The absorbed radiation for shaded leaves and each sunlit leaf with a particular orientation in each canopy layer was then used to scale photosynthesis from leaves to the whole-canopy (De Pury & Farquhar 1997).

ii) Net photosynthesis per unit of leaf area, A_n , was modelled via Michaelis–Menten type dependence upon CO₂ concentration in the mesophyll (Farquhar *et al.* 1980). The kinetic variables were parameterized using temperature response functions (Medlyn *et al.* 2002; Bernacchi *et al.* 2003) and empirical relationships among maximum carboxylation velocity ($V_{c,max}$), maximum rate of electron transport (J_{max}) and leaf dark respiration (R_d) (Walker *et al.* 2014; Atkin *et al.* 2015). Intercellular CO₂ concentration was computed from ambient CO₂ concentration via Fick's law and stomata conductance g_s to express $A_n = A_n(g_s)$.

iii) A stomata optimization scheme coupled with a hydraulic model was implemented to represent stomata response to light, vapor pressure deficit and soil water potential on the condition of carbon gain maximization, formulated as

$$(4) \quad \max_{g_s}(A_n - \Theta)$$

where Θ is the cost of water consumption (Cowan & Farquhar 1977; Katul *et al.* 2010). In order to account for costs related to water stress (e.g., embolism and dehydration), Θ was parameterized as function of leaf water potential ψ_L (Mpa). Theoretical studies suggest that Θ is a concave-up function (Sperry *et al.* 2016; Wolf *et al.* 2016); here for simplicity, we used a quadratic function (i.e., $\Theta = c_0\psi_L^2$, where c_0 is an empirical constant). ψ_L is obtained as a top boundary condition of a plant hydraulic system with a flow rate per unit of leaf area, F (mmol m⁻² s⁻¹), equal to $g_s(e_s(t_c) - e_a)$. Three idealized units comprise the plant hydraulic system: absorbing roots, transport element and evaporative surface (Appendix 2, Fig S3). The absorbing roots uptake water from soil at different depths and connect to the bottom of the transport element. They are represented as resistors in parallel according to

$$(5) \quad F = k_R \frac{1}{a_L} \sum_i a_{r,i} (\psi_{s,i} - \psi_0)$$

where k_R is the root membrane conductivity (mmol m⁻² s⁻¹ Mpa⁻¹), a_L is the plant leaf area (m²), $a_{r,i}$ is the absorbing root surface area in the i^{th} soil layer (m²), $\psi_{s,i}$ is the soil water potential in the i^{th} layer and ψ_0 the water potential at the bottom of the transport element. Form (5) we defined a total root conductivity per unit of leaf area $K_R = k_R \frac{1}{a_L} \sum_i a_{r,i}$. The flow in the transport element, which include transporting roots, main stem and branches, is calculated by integrating Darcy law along the hydraulic path

$$(6) \quad F = \int_{\psi_x + p_z}^{\psi_0} K_X(\psi) d\psi$$

where $k_x(\psi)$ is the whole-element xylem conductance per unit of plant leaf area (mmol m⁻² s⁻¹ Mpa⁻¹), ψ_x and p_z (Mpa) are the water potential and the hydrostatic pressure at the top of the transporting element, respectively. Similarly, the water flow through the evaporative surface is computed as:

$$(7) \quad F = \int_{\psi_L + p_z}^{\psi_X + p_z} K_L(\psi) d\psi$$

where K_L is the leaf conductance ($\text{mmol m}^{-2} \text{s}^{-1} \text{Mpa}^{-1}$). $K_X(\psi)$ and $K_L(\psi)$ attain a maximum value $K_{X,\text{max}}$ and $K_{L,\text{max}}$, respectively, for $\psi = 0$, and decreases for negative plant water potentials following a two-parameters sigmoidal vulnerability curve, defined by the water potentials corresponding to a 50% loss in conductivity ($p_{X,50}$ and $p_{L,50}$) and the slope at the inflection point. The model also assumed that $K_{X,\text{max}}$ is constant along the canopy profile. From a hydraulic perspective, this can be thought of as each leaf been independently connected to the soil by a conduit of equal maximum conductance. Eq. (5-7) with the maximization condition (4) constitute a closed system that can be solved numerically to find the optimal g_s . Canopy conductance g_c was evaluated by integrating the transpiration of each leaf across the canopy profile and dividing by $e_s(t_c) - e_a$, thus comparable to g_c computed from the eddy covariance tower, except for the contribution of soil evaporation (see above).

Model parametrization

The model was run at 5-min intervals for 2016-2017 when all observations to drive the model were available. These included: direct and diffuse PAR, canopy temperature, air humidity, soil moisture measurements at 10, 40 and 100 cm. The soil was discretized in four layers (0-10, 10-40, 40-100 and >100) and ψ_s of each layer computed from soil moisture with an empirical soil retention curve calibrated from data collected on an adjacent plot in 2015 and 2016 (Kupers *et al.* 2019). The last layer (>100 cm) was considered to have a constant ψ_s . Root distribution followed the exponential decay (parameter in table 1 of Jackson *et al.* 1996). The solar zenith angle for the radiative transfer model was computed using the algorithm in Andreas (2003). The forest was discretized in 10 vertical layers of equal leaf area, and, in each layer, eleven leaf classes were defined: one shaded leaf and ten sunlit leaves with different orientations. Leaf gas exchange measurements collected on two forests along the Panama canal equipped with cranes with access to the canopy suggested that, on average, $V_{c,\text{max}}$ at reference temperature (25 °C) of a mature *canopy* leaf is about three times that of a mature *understory* leaf (Xu *et al.* 2017). Thus, $V_{c,\text{max}}$ was varied linearly within the canopy so its value at the top layer was three times that at the bottom layer. Leaf angle distribution was also varied along the canopy based on data collected from several towers in BCI, including the eddy covariance tower, indicating more vertical distributions in the canopy top and flatter in the understory (Detto *et al.* 2015). Leaf area index was varied between 5 and 6 in the dry and wet seasons, respectively, according to observations based on hemispherical photographs given in Detto *et al.* (2018). We also assumed coordination among hydraulic organs (Sack *et al.* 2003; Bartlett *et al.* 2016) and assigned $K_R = K_{x,\text{max}} = K_{L,\text{max}}$, given that, on average, leaf resistance is 30% of total plant resistance (Sack & Holbrook 2006). $V_{c,\text{max}}$ at the top of the canopy, the maximum hydraulic conductances and c_0 , which are the critical parameters that express the plant sensitivity to water stress, were kept as free parameters. The sensitivity of the model to these parameters were explored in a series of simulations. The other two parameters of the vulnerability curve were obtained from measurements of stem conductivity of 26 tree Panamanian species (data available in Wolfe *et al.* 2021). $p_{L,50}$ was assumed to be %60 of $p_{L,50}$ (Scoffoni & Sack 2017). For other model parameters see Appendix 2: Table S1. Code available online.

Results

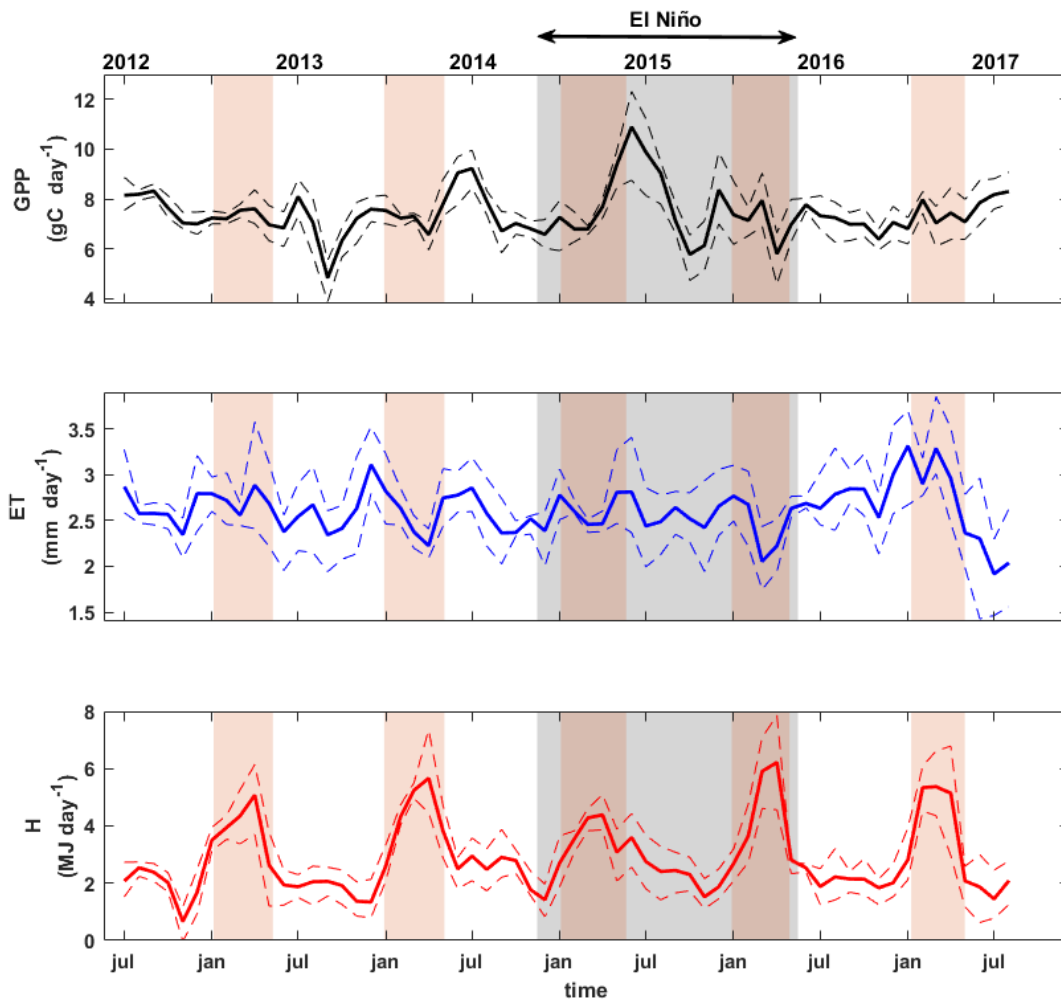


Figure 2. Daily fluxes of gross primary productivity (GPP), evapotranspiration (ET) and sensible heat (H) averaged by month, derived from eddy covariance measurements on Barro Colorado Island between 2012 and 2017. Dashed lines bound the interquartile range of daily fluxes for each month. Red shaded areas indicate the dry seasons and the dark shaded area delimits the El Niño event as defined by the Oceanic Niño Index.

GPP and ET monthly series did not display any evident long-term trend or seasonality, although ET is on average $\sim 12\%$ higher during the dry season (Fig. 2). The most apparent pattern was the high GPP at the beginning of the 2015 wet season during El Niño, a pattern that was not present in ET. In contrast, H displays strong seasonality with a peak in the dry season.

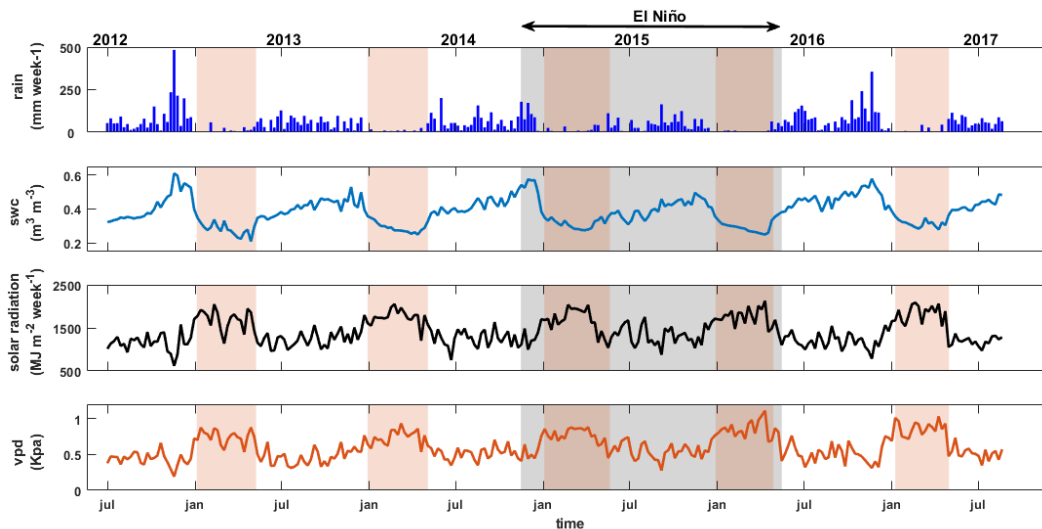


Figure 3. Principal hydro-meteorological drivers observed on Barro Colorado during the study period at a weekly time scale. Red shaded areas indicate the dry seasons and the dark shaded area delimits El Niño event as defined by the Oceanic Niño Index.

The principal hydro-climatic drivers show the typical pattern of a seasonal tropical climate, with a pronounced but short dry season (Figure 3). Precipitation displays large temporal variability at interannual, seasonal, and intra-seasonal time scales with frequent dry spells ranging from few days to several weeks, especially in the 2016 dry season during the last phase of the El Niño. The 2015 wet season appeared to be less wet than the others and was characterized by two unusual dry spells in June and July. Note how the weekly series of solar radiation and D were highly correlated.

The two anomalous dry spells in the 2015 wet season are shown with more resolution in Figure 4. These events lasted 28 and 15 days, respectively, neglecting some occasional small rainfalls that did not produce any detectable fluctuation in the surface soil moisture (Figure 4c). GPP increased during the spells, reaching almost 15 gC per day with an interesting linear increase pattern and an abrupt drop at the end of the spell, especially evident in the second one (Figure 4a). Higher solar radiation, a consequence of the relatively cloud-free sky during the spells, could partially explain the productivity bursts. Note also that the vapor pressure deficit was not particularly high (Figure 4d).

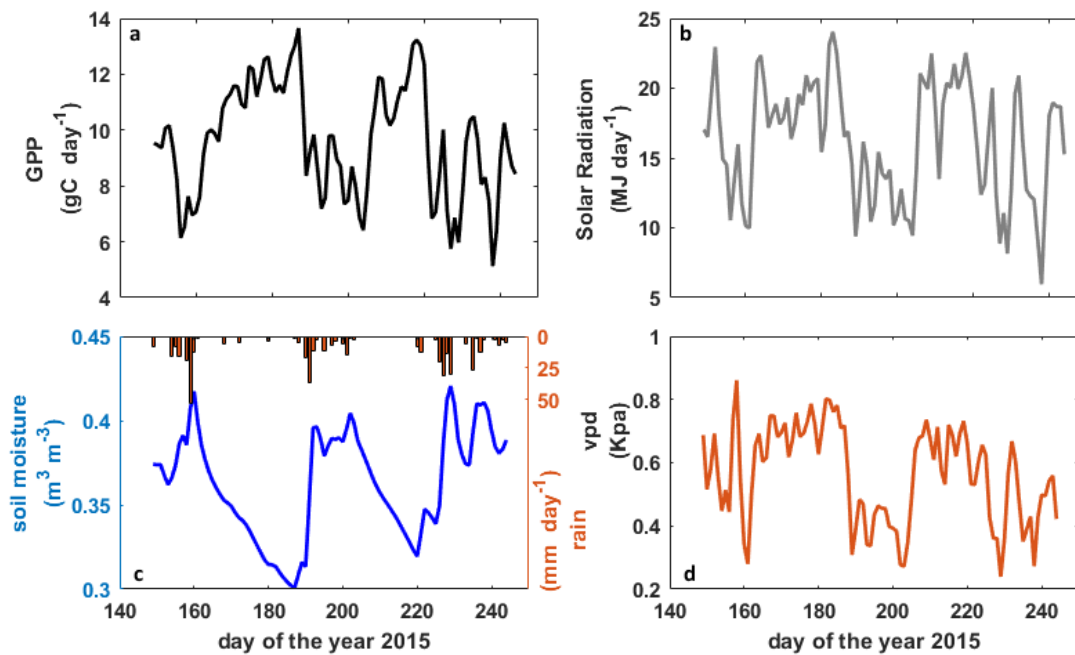


Figure 4. Daily values of GPP (a), solar radiation (b), soil moisture and rainfall (c), and vapor pressure deficit (d) during the two dry spells that hit BCI in the 2015 El Niño. All daily values (except for rainfall) are computed using a 2-day moving window.

To understand the ecosystem behavior in terms of water and carbon fluxes, we explored two basic ecosystem functions: the light-use and the water-use efficiencies (Figure 5). We performed separate analyses for wet and dry seasons (see method). The light-use efficiency shows saturation at intermediate levels of PAR. The curves clearly separate between the two seasons, with the wet season yielding more carbon for each PAR level. Interestingly, the water use efficiency was higher during the wet season.

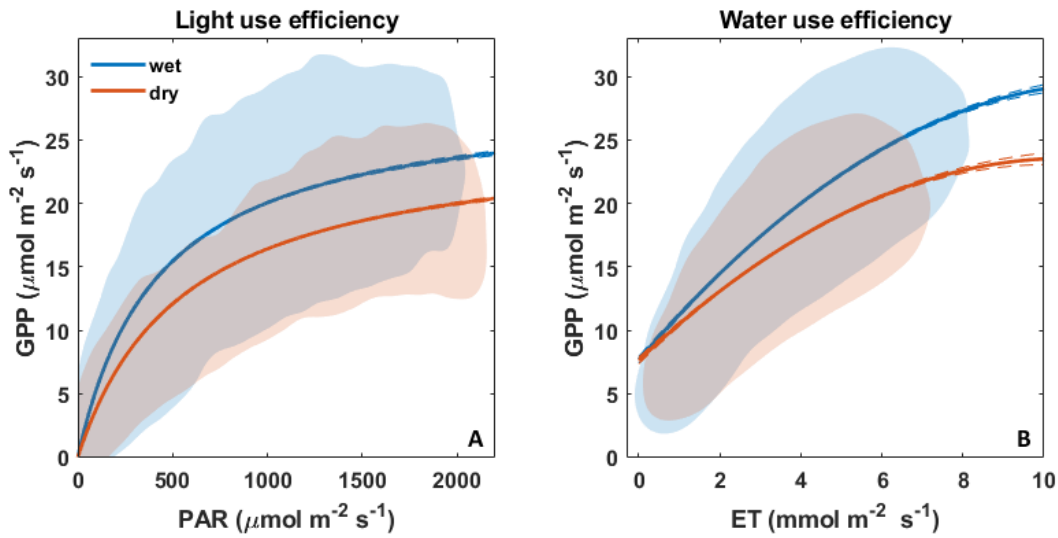


Figure 5. A) Light use efficiency and B) water use efficiency for the wet and dry season. Shaded areas enclose 75% of the observations (see method for further details on the analyses). Model regression lines, a Michaelis-Menten in A and a quadratic equation in B, with 95% confidence intervals are shown as a reference.

The response of canopy conductance, g_c , to environmental stimuli provided further insights. When plotted against the combination of terms $\frac{A}{c_a \sqrt{D}}$, g_c displays, in the majority of the cases, an approximately linear increase consistent with leaf physiological response (Figure 6). Except for few overlapping curves in the wet season, the data separate well according to soil moisture regimes in both seasons. In general, g_c was higher in the wet season. Interestingly, g_c during the dry season had lower sensitivity (flatter slopes) for drier conditions.

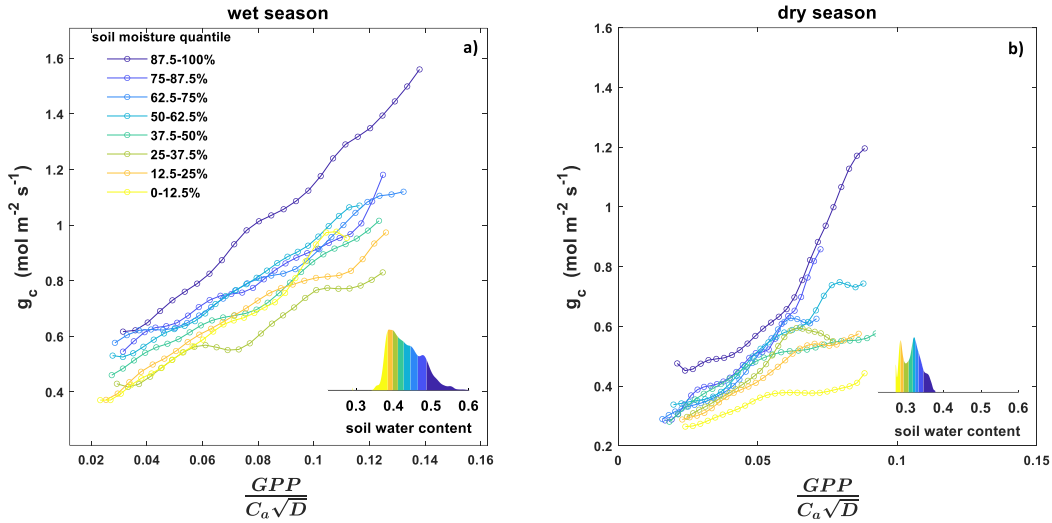


Figure 6. The dependence of surface (canopy) conductance to vapor pressure deficit varies with soil moisture depending on the season. The relationship between surface conductance (g_c), and the combination of terms ($GPP \text{ Ca}^{-1} \text{ D}^{-1/2}$) changes with surface soil moisture regimes. Circles show kernel density estimations of g_c within unique soil moisture bins. The insets show the soil moisture distributions for each season divided into quantiles by color (see methods for further details).

The model, implemented with the coupled hydraulic-stomata optimization, was able to reproduce the observed patterns of g_c , with different responses to D according to soil moisture regimes (Figure 7), especially in the dry season. The slopes are flatter for drier conditions in Figure 7b. For this simulation model parameters were tuned so minimum values of ψ_L were in the range of midday ψ_L measured on several canopy species during the high of the dry season (Wright & Cornejo 1990) Figure 7c.

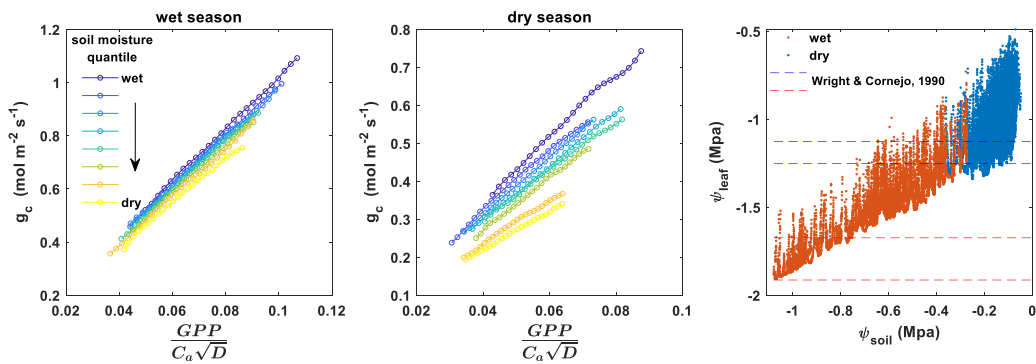


Figure 7. The relationship between surface conductance (g_c), and the combination of terms ($GPP \text{ Ca}^{-1} \text{ D}^{-1/2}$) from a multilayer photosynthesis model coupled with plant hydraulics for the same hydro-climate conditions of Fig. 6 during wet (a) and dry (b) season. In (c) the relationship between soil water potential and average top of the canopy ψ_L . Dashed lines bounds measurements of midday ψ_L (mean \pm SE) from Wright & Cornejo (1990) for wet (-) and dry (-) season. Model parameters: $V_{c,\max} = 40 \mu\text{mol m}^{-2} \text{ s}^{-1}$, $k_{L,\max} = 20 \text{ mmol m}^{-2} \text{ s}^{-1} \text{ Mpa}^{-1}$, $c_0 = 1 \mu\text{mol m}^{-2} \text{ s}^{-1} \text{ Mpa}^{-2}$ (for other parameters see methods and Appendix 2).

The following analyses explore the model's sensitivity to the key-study parameters, including LAI, $V_{c,max}$ at the canopy top, $K_{L,max}$, and the cost coefficient c_0 , for typical midday conditions during wet and dry seasons. For each combination of parameters, we compute net photosynthesis ($A_n = \text{GPP} - \text{leaf dark respiration}$) and $A_{net} - \Theta$, representing the available carbon after paying the cost of water.

For LAI and $V_{c,max}$, i.e. leaf quantity and quality, the model is, in general, more sensitive $V_{c,max}$ than LAI, especially at low $V_{c,max}$ values (Figure 8, top panels). At high $V_{c,max}$, a maximum emerges due to high respiratory costs that result in negative carbon balance in shaded leaves because leaf dark respiration is proportional to $V_{c,max}$. In the dry season, the carbon gain is further penalized by the high cost of water resulting in a maximum at lower LAI (compare Figure 8b and 8d). In general, the model also predicts lower midday photosynthesis during the dry season, consistent with the observed mean diurnal variation of GPP (suppl. material Fig. S8).

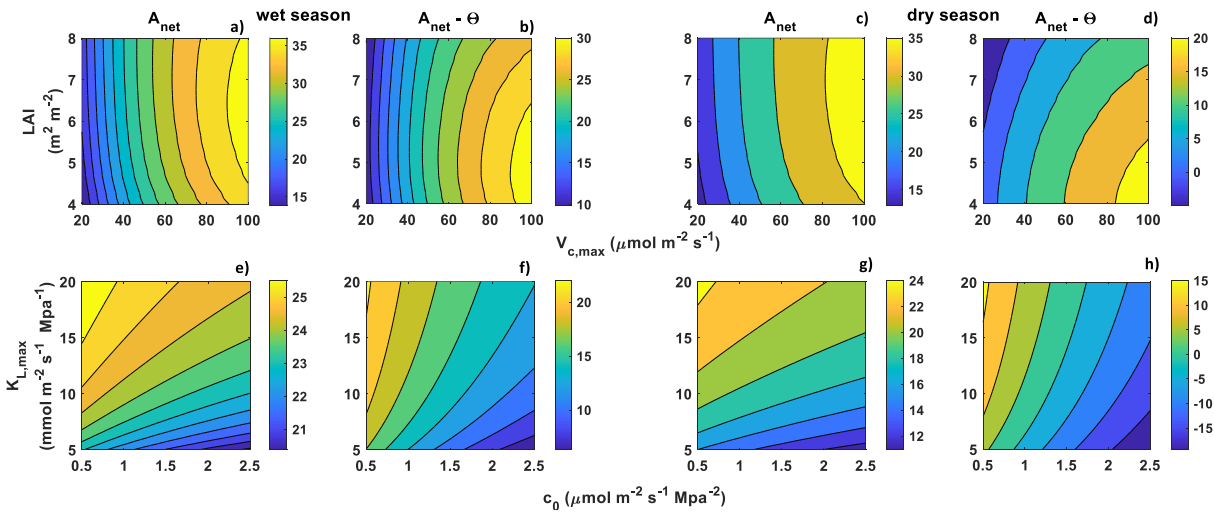


Figure 8. Model parameters exploration. Contour plots of net photosynthesis, $A_{net} = \text{GPP} - \text{leaf dark respiration}$ (a, c, e, and g) and net photosynthesis minus water carbon cost Θ (b, d, f and h) for typical midday conditions during wet (left panels) and dry (right panels) seasons. Top panels, different combinations of LAI and $V_{c,max}$, with $c_0 = 1 \mu\text{mol m}^{-2} \text{s}^{-1} \text{Mpa}^{-2}$, $K_{L,max} = 1 \text{mmol m}^{-2} \text{s}^{-1} \text{Mpa}^{-1}$ kept constant. Bottom panels, different combinations of $K_{L,max}$ and cost coefficient c_0 with LAI = 6 (wet) and 5 (dry) and $V_{c,max} = 40$ kept constant. Environmental variables [wet and dry season]: PAR = [1200 1700] $\mu\text{mol m}^{-2} \text{s}^{-1}$, $D = [0.5 \text{ } 0.8] \text{Kpa}$, $\psi_s = [-0.5 \text{ } -1.2] \text{Mpa}$.

The model is also quite sensitive to $K_{L,max}$ and c_0 , i.e., the efficiency of water transport and the cost of water stress, especially in the dry season (Figure 8, bottom panels). In the dry season, c_0 can generate negative carbon gain due to the high cost of water driven by the combination of high D and lower ψ_s (Figure 8h).

The sensitivity of the model to coupling atmospheric conditions is explored in the simulations presented in Figure 9. The simulations are conducted for different linear combinations of climatic conditions where D and PAR increase while ψ_s decreases, which qualitatively represent common patterns of co-varying

environmental factors. Figure 9 shows that it is possible to have a positive trend of GPP with increasing D for moderate soil drying conditions (blue and red lines). For fast rates of soil drying, GPP has a non-monotonic behavior, increasing in the first phase of the drought and declining sharply later (yellow lines). Note the large sensitivity of the model to plant hydraulic conductance (compare continuous and dashed lines). A lower conductance generates a faster decline of GPP with water stress.

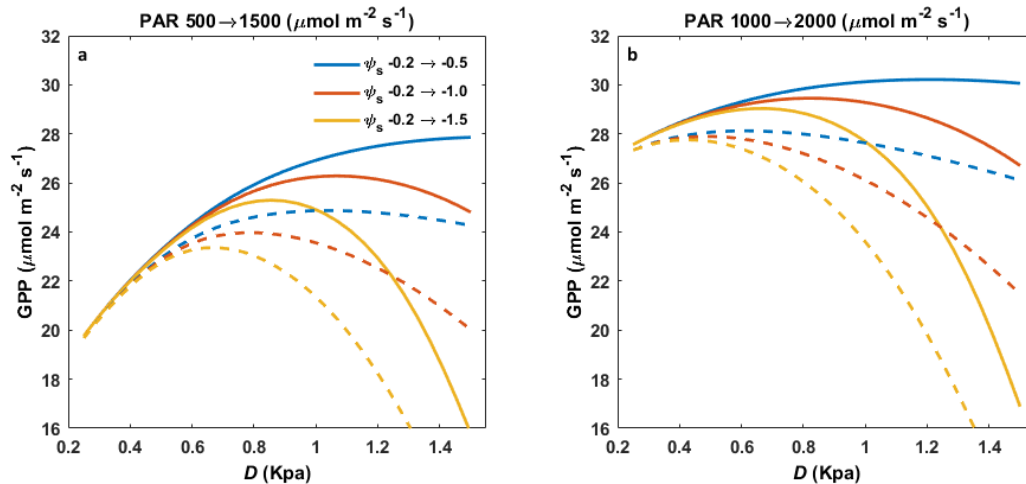


Figure 9. Model simulations of increasing water stress for coupled climatic conditions. The curves depict GPP as function of water vapor deficit (D) when PAR increases linearly with D and simultaneously soil water potential decreases linearly with D . The two panels are for different ranges of PAR. In **a**) PAR was varied between 500 and 1500 ($\mu\text{mol m}^{-2} \text{s}^{-1}$), in **b**) PAR was varied between 1000 and 2000 ($\mu\text{mol m}^{-2} \text{s}^{-1}$). Different colors represent different soil drying conditions: in blue soil water potential was varied between -0.2 to -0.5 Mpa, in red from -0.2 to -1 Mpa, and in yellow from -0.2 to -1.5 Mpa. The simulations are performed for two values of maximum whole-plant hydraulic conductance per unit of leaf area, K_{max} equal 2 and 1 $\text{mmol m}^{-2} \text{s}^{-1} \text{Mpa}^{-1}$ (continuous and dashed lines, respectively).

Discussion

Empirical patterns

This part of the tropics is characterized by a relatively short but intense dry season and strong interannual variability, caused mainly by ENSO. Despite the seasonal climate and phenology, the lack of seasonality in the GPP and ET temporal patterns indicates compensatory processes are operating in this forest. The analyses of basic ecosystem functions, such as light and water use efficiency, revealed distinct behaviors among the two seasons. Physiological controls appear to be the most likely explanation for these patterns, as suggested by the interacting response of canopy conductance to vapor pressure deficit and soil moisture.

Qualitatively, the seasonal differences in GPP for the same PAR level and water transpired can be explained by two factors. On the one hand, higher atmospheric demand and lower water supply during

the dry season cause a reduction in LAI and a strong stomata regulation to alleviate stress on the plant hydraulic system by relieving some of the xylem tension. On the other hand, higher solar radiation, especially in the afternoon when cloudiness is more frequent in the wet season, compensates for the negative effects of water stress (reduced midday peak), resulting in an equal daily GPP between the seasons (suppl. mat. Fig. S8). A secondary effect that might contribute to higher use efficiency during the wet season is a larger fraction of diffuse radiation, which plants use more efficiently (Roderick *et al.* 2001). However, direct measurements of PAR components showed higher direct radiations during the dry season, but the diffuse component was very similar among seasons (suppl. mat. Fig. S9), so we exclude this hypothesis.

One of the surprising patterns was the hydrological control of g_c during the wet season when soil moisture was not limiting. This result can be explained by the large fluctuations of the surface soil moisture (the analyses used the top 15 cm) during the wet season because of the alternation of wetting and drying phases. In this tropical forest, plants allocate most of the fine absorbing roots in the top layer to maximize nutrient acquisition, especially nitrogen (Cavelier 1992). Consequently, fluctuations in surface soil moisture can reflect in the plant water potential. Another surprising result was the increase of GPP during El Niño, a pattern that was not documented in a previous study (Fang *et al.* 2021); see below for more discussion.

Modeling analyses

Model results corroborated these empirical patterns. In fact, despite the simplified representation of the hydraulic system, the model could reproduce the observed trends in g_c . Although water storage, the complexity of the hydraulics system (i.e., the flow through different organs with different hydraulic properties) have been shown to be important aspects of the plant response to water stress (e.g., Meinzer *et al.* 2003; Christoffersen *et al.* 2016), these results suggest that the key to model hydraulically-mediated water stress lies in the interactions between the cost of moving water and the efficiency of water transport. This results in a water shadow price - often referred as λ (Cowan & Farquhar 1977; Katul *et al.* 2010), which is a function of plant hydraulic state, ψ_L . In particular, it can be shown that λ is the ratio between the marginal cost and the efficiency in water transport (i.e., how much additional carbon the plant pays and how much additional water is moved for a decrease of a unit of ψ_L).

Unfortunately, our understanding of the cost function is less developed than the functions regulating water transport, although recent studies have made some progress in this direction (Brodersen *et al.* 2018; Klein *et al.* 2018). Assuming the cost as a simple quadratic function of leaf water potential (i.e., $\Theta = c_0 \psi_L^2$) is convenient for the model economy as it avoids introducing another parameter describing the nonlinearity and was sufficient to reproduce the patterns and consistent with some theoretical studies suggested that the form of this function is concave up (Sperry *et al.* 2016; Wolf *et al.* 2016). A different nonlinear form might have produced more pronounced differences in the response of g_c to soil moisture in the wet season (Figure 7a). Furthermore, the exact form of the cost function will be important for estimating the whole-plant carbon budget, which are usually not account for in current ecosystem models. Our model simulations show that accounting for these costs generate different

sensitivities to model parameters (panels b, d, f and h in Fig. 8), which will be crucial to understanding the long-term effects of water stress in tropical forests and shifts in hydraulic traits (Bartlett *et al.* 2019).

Model results also suggest that reduced LAI in the dry season does not significantly cause a loss in productivity, as thinning the canopy layer stimulates understory productivity, in agreement with observed dynamics of Lidar-derived forest structures observed over the Amazon (Tang & Dubayah 2017). Although we do not have direct observations of changes in leaf chemical and photosynthetic properties or timing of leaf flushing, previous analyses of temporal patterns of leaf fall (Detto *et al.* 2018) and inspection of phenocam images suggest that the several canopy trees flush new leaves preferentially at the transition between dry and wet season, although a plethora of species phenological strategies coexist in this forest including dry season flush (Wright 1996). This suggests that the canopy has a high potential photosynthetic capacity at the beginning of the wet season. Furthermore, if the soil water reservoirs have been fully replenished during this period, variation in solar radiation can determine large interannual variability in forest GPP. This series of events caused the burst in productivity in the 2015 El Niño during June and July as the two dry spells responsible for the increased GPP occurred well into the wet season after soil moisture recharged. The stronger role of $V_{c,max}$ compared to LAI will have critical implications for ecosystem model developments of tropical forests as it would be more important to correctly represent changes in leaf photosynthetic properties rather than LAI seasonality. However, representing these seasonal and interannual variations will be challenging as it involves tracking leaves ontogenetic processes (Detto & Xu 2020) and timing of flushing and shedding (Wu *et al.* 2016).

Comparison with other studies

The strong canopy conductance response to water stress agrees with other ecosystem-scale studies in tropical forests (Aguilos *et al.* 2018; Barros *et al.* 2019) and could also explain the lack of pattern in the leaf-gas exchange study of Wu *et al.* (2020). Wu *et al.* (2020) found no support for the stomata-mediated hydraulic hypothesis as there were no differences in stomatal response to water stress (specifically the slope of the g_s with D as in Figure 7) in two forests across the Panamanian rainfall gradient and weak effect of ψ_L . Although our study was conducted in a single forest, we show that the hydraulic control is present in both, the wet and in the dry season. If time could be traded for space, our results predict that response to water stress of forests with different precipitation regimes might not be very different. As we have mentioned above, the shadow price λ , which is equivalent to the slope of the curves in Fig. 7 (Medlyn *et al.* 2011), is a ratio of two plant properties: the marginal cost and efficiency of moving water. It is likely that there is a tradeoff between these two properties, as plants with an efficient hydraulic system (usually in wetter forest) pay also a greater price under water stress. This will equalize stomata response among forests that differs in hydraulic traits, consistent with the conclusion in Barros *et al.* (2019).

Although leaf-gas exchange studies provide invaluable knowledge about the functional diversity of tropical forests, there are challenges in integrating leaf-level processes into an ecosystem response. Eddy covariance studies have advantages and disadvantages in this regard. First, they integrate the

response to the whole ecosystem; unfortunately, they also include other confounding factors such as soil evaporation and systematic errors (see below). Another crucial advantage is that fluxes are observed quasi-continuously throughout the year, allowing exploring a wider range of environmental variability than intense but sporadic field campaigns.

To our best knowledge, a few studies documented the effect of El Niño on GPP using eddy covariance in tropical forests. Cavaleri *et al.* (2017) reported a decline in carbon sink (lower GPP and higher ecosystem respiration) in a Costa Rican forest during the 1998 event caused by warming and drying. These results agreed with another Costa Rican forest located in a drier part of the country in relation to the 2015 event (Castro *et al.* 2018). In contrast, Olchev *et al.* (2015) found an increase of ET and GPP in an Indonesian forest attributed to higher solar irradiance during two moderate ENSO events between 2004 and 2008. Stiegler *et al.* (2019) presented a more complex picture in a study on an oil palm plantation in Sumatra during the 2015 event. In the first part of the drought, GPP increased despite a sharp depletion of surface soil moisture and increased VPD. However, a decline in GPP was observed in the second part of the event, attributed to an emerging smoke haze that decreased incoming solar radiation. A reduction of GPP and ET was also observed in a secondary dry dipterocarp forest in Thailand during the 2015 event (Kaewthongrach *et al.* 2020). The reduction was attributed to an earlier leaf shedding of the dipterocarps. A two-year study in the *Caatinga* biome (northeastern Brazil) found a reduction of carbon sink during 2015 compared to the previous wetter year (Mendes *et al.* 2020). Our study is consistent with the net positive effect of reduced cloud cover.

Uncertainty in flux partitioning

One of the complications of analyzing eddy covariance data is the uncertainty related to partitioning NEE into GPP and ecosystem respiration, a problem common in forest ecosystems (Loescher *et al.* 2006; Speckman *et al.* 2015). This problem is present at our site as ecosystem respiration appeared to be underestimated compared with soil respiration measurements conducted in the tower footprint using a combination of manual and automated chambers (Rubio & Detto 2017). The quantification of flux underestimation and systematic errors is still an active area of research (Hayek *et al.* 2018), especially in tropical ecosystems with tall and dense vegetation (Fu *et al.* 2018).

Although this topic is outside the scope of the study, our measurements can provide some valuable insights. First, nighttime-derived respiration was lower than respiration derived from the intercept of the light use efficiency, which was more comparable to chamber-derived respiration (Supplementary Material – Fig. S4). Nighttime-derived respiration was computed using a relatively restricted filter (friction velocity $>0.4 \text{ m s}^{-1}$, compared to the rule-of-thumb $>0.1 \text{ m s}^{-1}$) indicating that low turbulent conditions were not the only factor contributing to the underestimation. Light use efficiency-derived respiration was still underestimated because ecosystem respiration comprises soil and all above-ground sources (stems and leaves), which can contribute up to 40-50% of total respiration (Malhi *et al.* 2011).

Interestingly, the CO_2 vertical profiles were relatively uniform from 10 to 30 m and increased sharply close to the ground (Supplementary Material – Fig. S5a), suggesting a decoupling of sub-canopy flow even during daytime (Jocher *et al.* 2018). Although the area surrounding the tower was relatively flat, it is located on a top plateau that could be subjected to drainage and advection fluxes. The storage term

computed from the CO₂ profiles also suggested this hypothesis because storage could only partially explain the missing contribution to respiration (storage accounted for about 10% of the CO₂ flux measured above the canopy, Fig. S5c). Unfortunately, the CO₂ profile measurements were available only for a limited period, and the storage term, computed on a 30 min interval, was too noisy to be included in the calculation of the fluxes.

Although this underestimation could, in turn, affect GPP (Barba *et al.* 2018), it should not have significantly altered the temporal patterns presented here. Ecosystem respiration was higher during the wet seasons despite lower wind conditions (Fig. S4), consistent with chamber measurements in Rubio & Detto (2017). This suggests that systematic errors did not vary systematically with seasons. The increase of GPP during the two dry spells in the El Niño year also appears robust because of a low percentage of gaps during that period (Fig. S1) and because the trend was also present in the NEE series, so it cannot be attributed to a bias in the partitioning. The lack of seasonality in GPP is also found in ET, but not in H, meaning that the eddy covariance can capture seasonal fluxes when they are present. Finally, the energy balance closure was comparable to closures within the Fluxnet sites (Wilson *et al.* 2002) with an imbalance of about 25%, and no appreciable differences between wet and dry seasons (Fig. S10).

Conclusions

This study shows a critical role of plant physiological response in understanding the temporal variation of ecosystem fluxes in tropical forests. Interestingly, lack of seasonality underpins different functional behaviors of the forest between the two seasons, with plants adopting a more water-conserving strategy in the period of higher water stress. Nonetheless, the plant hydraulic control operates ubiquitously in this forest.

The picture that emerges from the literature review and the temporal pattern of the present study suggests that the response of tropical forests to El Niño is a result of a combination of factors contingent on a particular forest. Although El Niño is the warming phase of a large climatic event with a period of 3-7 years, its impact on the hydrological cycle effects can be quite variable in different tropical areas (Solander *et al.* 2020) and can be determined by few sporadic events such as the occurrence of unusual dry spells. Thus, the duration and the timing of a dry spell in relation to the forest phenological cycle become critical. As the frequency and timing of the dry spells are predicted to be altered during climate change (Marengo *et al.* 2009; Singh *et al.* 2014), it will be important to understand better how different forests behave during these relatively small scales events.

Acknowledgments. We thank Pablo Ramos and Paulino Villareal for all the assistance with the maintenance of the tower. The eddy covariance flux tower was funded by ForestGEO (Smithsonian). MD was supported by the Carbon Mitigation Initiative at Princeton University and NSG grant 2017804.

References (107)

- Aguilos, M., Hérault, B., Burban, B., Wagner, F. & Bonal, D. (2018). What drives long-term variations in carbon flux and balance in a tropical rainforest in French Guiana? *Agric. For. Meteorol.*, 253–254, 114–123.
- Atkin, O.K., Bloomfield, K.J., Reich, P.B., Tjoelker, M.G., Asner, G.P., Bonal, D., *et al.* (2015). Global

- variability in leaf respiration in relation to climate, plant functional types and leaf traits. *New Phytol.*, 206, 614–636.
- Barba, J., Cueva, A., Bahn, M., Barron-Gafford, G.A., Bond-Lamberty, B., Hanson, P.J., *et al.* (2018). Comparing ecosystem and soil respiration: Review and key challenges of tower-based and soil measurements. *Agric. For. Meteorol.*, 249, 434–443.
- Barkhordarian, A., Saatchi, S.S., Behrangi, A., Loikith, P.C. & Mechoso, C.R. (2019). A Recent Systematic Increase in Vapor Pressure Deficit over Tropical South America. *Sci. Rep.*, 9, 1–12.
- Barros, F. de V., Bittencourt, P.R.L., Brum, M., Restrepo-Coupe, N., Pereira, L., Teodoro, G.S., *et al.* (2019). Hydraulic traits explain differential responses of Amazonian forests to the 2015 El Niño-induced drought. *New Phytol.*, 223, 1253–1266.
- Bartlett, M.K., Detto, M. & Pacala, S.W. (2019). Predicting shifts in the functional composition of tropical forests under increased drought and CO₂ from trade-offs among plant hydraulic traits. *Ecol. Lett.*, 22, 67–77.
- Bartlett, M.K., Klein, T., Jansen, S., Choat, B. & Sack, L. (2016). The correlations and sequence of plant stomatal, hydraulic, and wilting responses to drought. *Proc. Natl. Acad. Sci. U. S. A.*, 113, 13098–13103.
- Bear, C., Reichstein, M., Tomelleri, E., Ciais, P., Jung, M., Carvalhais, N., *et al.* (2010). Terrestrial gross carbon dioxide uptake: global distribution and covariation with climate. *Science*, 329, 834–8.
- Bernacchi, C.J., Pimentel, C. & Long, S.P. (2003). In vivo temperature response functions of parameters required to model RuBP-limited photosynthesis. *Plant, Cell Environ.*, 26, 1419–1430.
- Bonal, D., Burban, B., Stahl, C., Wagner, F. & Hérault, B. (2016). The response of tropical rainforests to drought—lessons from recent research and future prospects. *Ann. For. Sci.*, 73, 27–44.
- Brodersen, C.R., Knipfer, T. & McElrone, A.J. (2018). In vivo visualization of the final stages of xylem vessel refilling in grapevine (*Vitis vinifera*) stems. *New Phytol.*, 217, 117–126.
- Brodribb, T.J., Powers, J., Cochard, H. & Choat, B. (2020). Hanging by a thread? Forests and drought. *Science (80-.)*, 266, 261–266.
- Brutsaert, W. & Sugita, M. (1991). A bulk similarity approach in the atmospheric boundary layer using radiometric skin temperature to determine regional surface fluxes. *Boundary-Layer Meteorol.*, 55, 1–23.
- Cai, W., Borlace, S., Lengaigne, M., Van Rensch, P., Collins, M., Vecchi, G., *et al.* (2014). Increasing frequency of extreme El Niño events due to greenhouse warming. *Nat. Clim. Chang.*, 4, 111–116.
- Carswell, F.E., Costa, A.L., Palheta, M., Malhi, Y., Meir, P., Costa, J.D.P.R., *et al.* (2002). Seasonality in CO₂ and H₂O flux at an eastern Amazonian rain forest. *J. Geophys. Res. Atmos.*, 107, LBA 43-1-LBA 43-16.
- Castro, S.M., Sanchez-Azofeifa, G.A. & Sato, H. (2018). Effect of drought on productivity in a Costa Rican tropical dry forest. *Environ. Res. Lett.*, 13.
- Cavaleri, M.A., Coble, A.P., Ryan, M.G., Bauerle, W.L., Loescher, H.W. & Oberbauer, S.F. (2017). Tropical rainforest carbon sink declines during El Niño as a result of reduced photosynthesis and increased respiration rates. *New Phytol.*

- Cavelier, J. (1992). Fine-root biomass and soil properties in a semideciduous and a lower montane rain forest in Panama. *Plant Soil*, 142, 187–201.
- Christoffersen, B.O., Gloor, M., Fauset, S., Fyllas, N.M., Galbraith, D.R., Baker, T.R., *et al.* (2016). Linking hydraulic traits to tropical forest function in a size-structured and trait-driven model (TFS v.1-Hydro). *Geosci. Model Dev.*, 9, 4227–4255.
- Christoffersen, B.O., Restrepo-Coupe, N., Arain, M.A., Baker, I.T., Cestaro, B.P., Ciais, P., *et al.* (2014). Mechanisms of water supply and vegetation demand govern the seasonality and magnitude of evapotranspiration in Amazonia and Cerrado. *Agric. For. Meteorol.*, 191, 33–50.
- Corlett, R.T. (2016). The Impacts of Droughts in Tropical Forests. *Trends Plant Sci.*, 21, 584–593.
- Cowan, I.R. & Farquhar, G.D. (1977). Stomatal function in relation to leaf metabolism and environment. *Symp. Soc. Exp. Biol.*, 31, 471–505.
- Crago, R.D. & Qualls, R.J. (2014). Use of land surface temperature to estimate surface energy fluxes: Contributions of Wilfried Brutsaert and collaborators. *Water Resour. Res.*, 50, 3396–3408.
- Croat, T.B. (1978). *Flora of Barro Colorado Island*. *Bull. Torrey Bot. Club*. Stanford University Press, Stanford.
- Detto, M., Asner, G.P., Muller-landau, H.C. & Sonnentag, O. (2015). Spatial variability in tropical forest leaf area density from multireturn lidar and modeling. *J. Geophys. Res.*, 294–309.
- Detto, M., Baldocchi, D. & Katul, G.G.G. (2010). Scaling Properties of Biologically Active Scalar Concentration Fluctuations in the Atmospheric Surface Layer over a Managed Peatland. *Boundary-Layer Meteorol.*, 136, 407–430.
- Detto, M., Wright, S.J., Calderón, O. & Muller-landau, H.C. (2018). Resource acquisition and reproductive strategies of tropical forest in response to the El Niño-Southern Oscillation. *Nat. Commun.*, 9, 1–8.
- Detto, M. & Xu, X. (2020). Optimal leaf life strategies determine $V_{c,max}$ dynamic during ontogeny. *New Phytol.*
- Eller, C.B., Rowland, L., Oliveira, R.S., Bittencourt, P.R.L., Barros, F. V., Da Costa, A.C.L., *et al.* (2018). Modelling tropical forest responses to drought and El Niño with a stomatal optimization model based on xylem hydraulics. *Philos. Trans. R. Soc. B Biol. Sci.*, 373.
- Fang, Y., Leung, L.R., Wolfe, B.T., Detto, M. & Knox, R.G. (2021). Disentangling the Effects of Vapor Pressure Deficit and Soil Water Availability on Canopy Conductance in a Seasonal Tropical Forest During the 2015 El Niño Drought. *J. Geophys. Res. Atmos.*, 1–20.
- Farquhar, G.D., Von Caemmerer, S. & Berry, J.A. (1980). A Biochemical Model of Photosynthetic CO_2 Assimilation in Leaves of C_3 Species. *Planta*, 149, 78–90.
- Feng, X., Porporato, A. & Rodriguez-iturbe, I. (2013). Changes in rainfall seasonality in the tropics. *Nat. Clim. Chang.*, 3, 811–815.
- Fu, Z., Gerken, T., Bromley, G., Araújo, A., Bonal, D., Burban, B., *et al.* (2018). The surface-atmosphere exchange of carbon dioxide in tropical rainforests: Sensitivity to environmental drivers and flux measurement methodology. *Agric. For. Meteorol.*, 263, 292–307.
- Goulden, M.L., Miller, S.D., Da Rocha, H.R., Menton, M.C., De Freitas, H.C., E Silva Figueira, A.M., *et al.*

- (2004). Diel and seasonal patterns of tropical forest CO₂ exchange. *Ecol. Appl.*, 14, 42–54.
- Green, J.K., Berry, J., Ciais, P., Zhang, Y. & Gentine, P. (2020). Amazon rainforest photosynthesis increases in response to atmospheric dryness. *Sci. Adv.*, In press, 1–10.
- Grossiord, C., Christoffersen, B., Alonso-Rodríguez, A.M., Anderson-Teixeira, K., Asbjornsen, H., Aparecido, L.M.T., *et al.* (2019). Precipitation mediates sap flux sensitivity to evaporative demand in the neotropics. *Oecologia*, 191, 519–530.
- Hagan, M.T. & Menhaj, M.. (1994). Training feedforward networks with the Marquardt algorithm. *IEEE Trans. Neural Networks*, 5, 989–993.
- Hayek, M.N., Wehr, R., Longo, M., Hutrya, L.R., Wiedemann, K., Munger, J.W., *et al.* (2018). A novel correction for biases in forest eddy covariance carbon balance. *Agric. For. Meteorol.*, 250–251, 90–101.
- Houghton, R. a. (2005). Aboveground Forest Biomass and the Global Carbon Balance. *Glob. Chang. Biol.*, 11, 945–958.
- Huang, M., Xu, Y., Longo, M., Keller, M., Knox, R.G., Koven, C.D., *et al.* (2020). Assessing impacts of selective logging on water, energy, and carbon budgets and ecosystem dynamics in Amazon forests using the Functionally Assembled Terrestrial Ecosystem Simulator. *Biogeosciences*, 17, 4999–5023.
- Jackson, R.B., Canadell, J., Ehleringer, J.R., Mooney, H.A., Sala, O.E. & Schulze, E.D. (1996). A global analysis of root distributions for terrestrial biomes. *Oecologia*, 108, 389–411.
- Jarvis, P.G. (1976). The interpretation of the variations in leaf water potential and stomatal conductance found in canopies in the field. *Philos. Trans. R. Soc. London. B, Biol. Sci.*, 273, 593–610.
- Jocher, G., Marshall, J., Nilsson, M.B., Linder, S., De Simon, G., Hörnlund, T., *et al.* (2018). Impact of Canopy Decoupling and Subcanopy Advection on the Annual Carbon Balance of a Boreal Scots Pine Forest as Derived From Eddy Covariance. *J. Geophys. Res. Biogeosciences*, 123, 303–325.
- Kaewthongrach, R., Chidthaisong, A., Charuchittipan, D., Vitasse, Y., Sanwangsri, M., Varnakovid, P., *et al.* (2020). Impacts of a strong El Niño event on leaf phenology and carbon dioxide exchange in a secondary dry dipterocarp forest. *Agric. For. Meteorol.*, 287.
- Katul, G., Manzoni, S., Palmroth, S. & Oren, R. (2010). A stomatal optimization theory to describe the effects of atmospheric CO₂ on leaf photosynthesis and transpiration. *Ann. Bot.*, 105, 431–442.
- Keller, M., Alencar, A., Asner, G.P., Braswell, B., Bustamante, M., Davidson, E., *et al.* (2004). Ecological research in the Large-scale Biosphere-Atmosphere Experiment in Amazonia: Early results. *Ecol. Appl.*, 14, 3–16.
- Klein, T., Zeppel, M.J.B., Anderegg, W.R.L., Bloemen, J., De Kauwe, M.G., Hudson, P., *et al.* (2018). Xylem embolism refilling and resilience against drought-induced mortality in woody plants: processes and trade-offs. *Ecol. Res.*, 33, 839–855.
- Koven, C., Knox, R., Fisher, R., Chambers, J., Christoffersen, B., Davies, S., *et al.* (2019). Benchmarking and Parameter Sensitivity of Physiological and Vegetation Dynamics using the Functionally Assembled Terrestrial Ecosystem Simulator (FATES) at Barro Colorado Island, Panama. *Biogeosciences Discuss.*, 1–46.
- Kupers, S.J., Wirth, C., Engelbrecht, B.M.J. & Rüger, N. (2019). Dry season soil water potential maps of a

- 50 hectare tropical forest plot on Barro Colorado Island, Panama. *Sci. Data*, 6, 1–9.
- Lasslop, G., Reichstein, M., Detto, M., Richardson, A.D. & Baldocchi, D.D. (2010). Comment on Vickers et al.: Self-correlation between assimilation and respiration resulting from flux partitioning of eddy-covariance CO₂ fluxes. *Agric. For. Meteorol.*, 150, 312–314.
- Loescher, H.W., Law, B.E., Mahrt, L., Hollinger, D.Y., Campbell, J. & Wofsy, S.C. (2006). Uncertainties in, and interpretation of, carbon flux estimates using the eddy covariance technique. *J. Geophys. Res. Atmos.*, 111, 1–19.
- Malhi, Y., Doughty, C. & Galbraith, D. (2011). The allocation of ecosystem net primary productivity in tropical forests. *Philos. Trans. R. Soc. B Biol. Sci.*, 366, 3225–3245.
- Marengo, J.A., Jones, R., Alves, L.M. & Valverde, M.C. (2009). Future change of temperature and precipitation extremes in south america as derived from the precis regional climate modeling system. *Int. J. Climatol.*, 29, 2241–2255.
- Martínez Cano, I., Shevliakova, E., Malyshev, S., Wright, S.J., Detto, M., Pacala, S.W., et al. (2020). Allometric constraints and competition enable the simulation of size structure and carbon fluxes in a dynamic vegetation model of tropical forests (LM3PPA-TV). *Glob. Chang. Biol.*, 1–17.
- Mauder, M., Cuntz, M., Drüe, C., Graf, A., Rebmann, C., Schmid, H.P., et al. (2013). A strategy for quality and uncertainty assessment of long-term eddy-covariance measurements. *Agric. For. Meteorol.*, 169, 122–135.
- Meador, W.E. & Weaver, W.R. (1980). Two-stream approximation to radiative transfer in planetary atmospheres: a unified description of existing methods and a new improvement. *J. Atmos. Sci.*, 37, 630–643.
- Medlyn, B.E., Dreyer, E., Ellsworth, D., Forstreuter, M., Harley, P.C., Kirschbaum, M.U.F., et al. (2002). Temperature response of parameters of a biochemically based model of photosynthesis. II. A review of experimental data. *Plant. Cell Environ.*, 25, 1167–1179.
- Medlyn, B.E., Duursma, R.A., Eamus, D., Ellsworth, D.S., Prentice, I.C., Barton, C.V.M., et al. (2011). Reconciling the optimal and empirical approaches to modelling stomatal conductance. *Glob. Chang. Biol.*, 17, 2134–2144.
- Meinzer, F.C., James, S.A., Goldstein, G. & Woodruff, D. (2003). Whole-tree water transport scales with sapwood capacitance in tropical forest canopy trees. *Plant, Cell Environ.*, 26, 1147–1155.
- Meir, P., Mencuccini, M. & Dewar, R.C. (2015). Drought-related tree mortality: Addressing the gaps in understanding and prediction. *New Phytol.*, 207, 28–33.
- Mendes, K.R., Campos, S., da Silva, L.L., Mutti, P.R., Ferreira, R.R., Medeiros, S.S., et al. (2020). Seasonal variation in net ecosystem CO₂ exchange of a Brazilian seasonally dry tropical forest. *Sci. Rep.*, 10, 1–16.
- Monteith J.I. (1965). Evaporation and environment. *Symp. Soc. Exp. Biol.*, 19, 205–234.
- Norman, J.M. (1980). Interfacing leaf and canopy light interception models. In: *Predicting Photosynthesis for Ecosystem Models*. CRC Press, Boca Raton, pp. 49–68.
- Novick, K.A., Ficklin, D.L., Stoy, P.C., Williams, C.A., Bohrer, G., Oishi, A.C., et al. (2016). The increasing importance of atmospheric demand for ecosystem water and carbon fluxes. *Nat. Clim. Chang.*, 6,

1023–1027.

- Olchev, A., Ibrom, A., Panferov, O., Gushchina, D., Kreilein, H., Popov, V., *et al.* (2015). Response of CO₂ and H₂O fluxes in a mountainous tropical rainforest in equatorial Indonesia to El Niño events. *Biogeosciences*, 12, 6655–6667.
- Pan, Y., Birdsey, R.A., Fang, J., Houghton, R., Kauppi, P.E., Kurz, W. a., *et al.* (2011). A large and persistent carbon sink in the world's forests. *Science*, 333, 988–993.
- Papale, D. & Valentini, R. (2003). A new assessment of European forests carbon exchanges by eddy fluxes and artificial neural network spatialization. *Glob. Chang. Biol.*, 9, 525–535.
- Pinty, B., Lavergne, T., Dickinson, R.E., Widlowski, J.L., Gobron, N. & Verstraete, M.M. (2006). Simplifying the interaction of land surfaces with radiation for relating remote sensing products to climate models. *J. Geophys. Res. Atmos.*, 111, 1–20.
- Poorter, L., McDonald, I., Alarcón, A., Fichtler, E., Licona, J.C., Peña-Claros, M., *et al.* (2010). The importance of wood traits and hydraulic conductance for the performance and life history strategies of 42 rainforest tree species. *New Phytol.*, 185, 481–492.
- Powers, J.S., Vargas G., G., Brodribb, T.J., Schwartz, N.B., Pérez-Aviles, D., Smith-Martin, C.M., *et al.* (2020). A catastrophic tropical drought kills hydraulically vulnerable tree species. *Glob. Chang. Biol.*, 26, 3122–3133.
- De Pury, D.G.G. & Farquhar, G.D. (1997). Simple scaling of photosynthesis from leaves to canopies without the errors of big-leaf models. *Plant, Cell Environ.*, 20, 537–557.
- Qian, X., Qiu, B. & Zhang, Y. (2019). Widespread Decline in Vegetation Photosynthesis in Southeast Asia Due to the Prolonged Drought During the 2015/2016 El Niño. *Remote Sens.*, 11, 910.
- Restrepo-Coupe, N., Levine, N.M., Christoffersen, B.O., Albert, L.P., Wu, J., Costa, M.H., *et al.* (2017). Do dynamic global vegetation models capture the seasonality of carbon fluxes in the Amazon basin? A data-model intercomparison. *Glob. Chang. Biol.*, 23, 191–208.
- Roderick, M., Farquhar, G., Berry, S. & Noble, I. (2001). On the direct effect of clouds and atmospheric particles on the productivity and structure of vegetation. *Oecologia*, 129, 21–30.
- Rubio, V.E. & Detto, M. (2017). Spatiotemporal variability of soil respiration in a seasonal tropical forest. *Ecol. Evol.*, 7.
- Rüger, N., Condit, R., Dent, D.H., DeWalt, S.J., Hubbell, S.P., Lichstein, J.W., *et al.* (2020). Demographic tradeoffs predict tropical forest dynamics. *Science (80-)*, 368, 165–168.
- Sack, L., Cowan, P.D., Jaikumar, N. & Holbrook, N.M. (2003). The “hydrology” of leaves: Co-ordination of structure and function in temperate woody species. *Plant, Cell Environ.*, 26, 1343–1356.
- Sack, L. & Holbrook, N.M. (2006). Leaf hydraulics. *Annu. Rev. Plant Biol.*, 57, 361–381.
- Santiago, L.S., Goldstein, G., Meinzer, F.C., Fisher, J.B., Machado, K., Woodruff, D., *et al.* (2004). Leaf photosynthetic traits scale with hydraulic conductivity and wood density in Panamanian forest canopy trees. *Oecologia*, 140, 543–550.
- Santos, V.A.H.F. dos, Ferreira, M.J., Rodrigues, J.V.F.C., Garcia, M.N., Ceron, J.V.B., Nelson, B.W., *et al.* (2018). Causes of reduced leaf-level photosynthesis during strong El Niño drought in a Central

- Amazon forest. *Glob. Chang. Biol.*, 24, 4266–4279.
- Scoffoni, C. & Sack, L. (2017). The causes and consequences of leaf hydraulic decline with dehydration. *J. Exp. Bot.*, 68, 4479–4496.
- Singh, D., Tsiang, M., Rajaratnam, B. & Diffenbaugh, N.S. (2014). Observed changes in extreme wet and dry spells during the south Asian summer monsoon season. *Nat. Clim. Chang.*, 4, 456–461.
- Solander, K.C., Newman, B.D., Carioca De Araujo, A., Barnard, H.R., Berry, Z.C., Bonal, D., *et al.* (2020). The pantropical response of soil moisture to El Niño. *Hydrol. Earth Syst. Sci.*, 24, 2303–2322.
- Speckman, H.N., Frank, J.M., Bradford, J.B., Miles, B.L., Massman, W.J., Parton, W.J., *et al.* (2015). Forest ecosystem respiration estimated from eddy covariance and chamber measurements under high turbulence and substantial tree mortality from bark beetles. *Glob. Chang. Biol.*, 21, 708–721.
- Sperry, J.S., Venturas, M.D., Anderegg, W.R.L., Mencuccini, M., Mackay, D.S., Wang, Y., *et al.* (2016). Predicting stomatal responses to the environment from the optimization of photosynthetic gain and hydraulic cost. *Plant. Cell Environ.*, In press.
- Stiegler, C., Meijide, A., Fan, Y., Ali, A.A., June, T. & Knohl, A. (2019). El Niño-Southern Oscillation (ENSO) event reduces CO₂ uptake of an Indonesian oil palm plantation. *Biogeosciences*, 16, 2873–2890.
- Tang, H. & Dubayah, R. (2017). Light-driven growth in Amazon evergreen forests explained by seasonal variations of vertical canopy structure. *Proc. Natl. Acad. Sci. U. S. A.*, 114, 2640–2644.
- Tyree, M.T., Cochard, H., Cruiziat, P., Sinclair, B. & Ameglio, T. (1993). Drought-induced leaf shedding in walnut: evidence for vulnerability segmentation. *Plant. Cell Environ.*, 16, 879–882.
- Walker, A.P., Beckerman, A.P., Gu, L., Kattge, J., Cernusak, L.A., Domingues, T.F., *et al.* (2014). The relationship of leaf photosynthetic traits - V_{max} and J_{max} - to leaf nitrogen, leaf phosphorus, and specific leaf area: A meta-analysis and modeling study. *Ecol. Evol.*, 4, 3218–3235.
- Watson, G.S. (1964). Smooth regression analysis. *Indian J. Stat.*, 26, 359–372.
- Wilson, K., Meyers, T., Goldstein, A., Baldocchi, D., Falge, E., Tenhunen, J., *et al.* (2002). Energy balance closure at FLUXNET sites. *Agric. For. Meteorol.*, 113, 223–243.
- Windsor, D.M. (1990). Climate and moisture variability in a tropical forest : long-term records from Barro Colorado Island, Panamá. *Smithson. Contrib. to Earth Sci.*, 29, 1–145.
- Wirth, R., Weber, B. & Ryel, R.J. (2001). Spatial and temporal variability of canopy structure in a tropical moist forest. *Acta Oecologica*, 22, 235–244.
- Wolf, A., Anderegg, W.R.L. & Pacala, S.W. (2016). Optimal stomatal behavior with competition for water and risk of hydraulic impairment. *Proc. Natl. Acad. Sci. U. S. A.*, 113, E7222–E7230.
- Wolfe, B., Cozzarelli, C.Y. & Jaén Barrios, N. (2021). *Stem hydraulic conductivity and vulnerability to cavitation for 26 tree species in Panama.*
- Wolfe, B.T., Sperry, J.S. & Kursar, T.A. (2016). Does leaf shedding protect stems from cavitation during seasonal droughts? A test of the hydraulic fuse hypothesis. *New Phytol.*, 212, 1007–1018.
- Wright, S.J. (1996). Phenological Responses to Seasonality in Tropical Forest Plants. In: *Tropical Forest Plant Ecophysiology* (eds. Mulkey, S.S., Chazdon, R.L. & Smith, A.P.). Chapman and Hall, New York, pp. 440–460.

- Wright, S.J. & Cornejo, F. (1990). Seasonal drought and Leaf Fall in a Tropical Forest. *Ecology*, 71, 1165–1175.
- Wright, S.J. & van Schaik, C.P. (1994). Light and the Phenology of Tropical Trees. *Am. Nat.*, 143, 192–199.
- Wu, J., Albert, L.P., Lopes, A.P., Restrepo-Coupe, N., Hayek, M., Wiedemann, K.T., *et al.* (2016). Leaf development and demography explain photosynthetic seasonality in Amazon evergreen forests. *Science*, 351, 972–6.
- Wu, J., Serbin, S.P., Ely, K.S., Wolfe, B.T., Dickman, L.T., Grossiord, C., *et al.* (2020). The response of stomatal conductance to seasonal drought in tropical forests. *Glob. Chang. Biol.*, 26, 823–839.
- Xu, X., Medvigy, D., Joseph Wright, S., Kitajima, K., Wu, J., Albert, L.P., *et al.* (2017). Variations of leaf longevity in tropical moist forests predicted by a trait-driven carbon optimality model. *Ecol. Lett.*, 20, 1097–1106.
- Xu, X., Medvigy, D., Powers, J.S., Becknell, J.M. & Guan, K. (2016). Diversity in plant hydraulic traits explains seasonal and inter-annual variations of vegetation dynamics in seasonally dry tropical forests. *New Phytol.*, 212, 80–95.
- Yan, J., Zhang, Y., Yu, G., Zhou, G., Zhang, L., Li, K., *et al.* (2013). Seasonal and inter-annual variations in net ecosystem exchange of two old-growth forests in southern China. *Agric. For. Meteorol.*, 182–183, 257–265.
- Yang, J. (2018). Amazon droughts and forest responses: Largely reduced forest photosynthesis but slightly increased canopy greenness during the extreme drought of 2015/2016. *Glob. Chang. Biol.*, 12, 3218–3221.
- Yuan, H., Dai, Y., Dickinson, R.E., Pinty, B., Shangguan, W., Zhang, S., *et al.* (2017). Reexamination and further development of two-stream canopy radiative transfer models for global land modeling. *J. Adv. Model. Earth Syst.*, 9, 113–129.
- Zhu, J., Zhang, M., Zhang, Y., Zeng, X. & Xiao, X. (2018). Response of Tropical Terrestrial Gross Primary Production to the Super El Niño Event in 2015. *J. Geophys. Res. Biogeosciences*, 123, 3193–3203.